

Simulating the characteristics of tropical cyclones over the South West Indian Ocean using a Stretched-Grid Global Climate Model

Molulaqhoob L. Maoyi¹ · Babatunde J. Abiodun¹ · Joseph M. Prusa² · Jennifer J. Veitch^{3,4}

Received: 3 July 2016 / Accepted: 21 April 2017 / Published online: 4 May 2017
© Springer-Verlag Berlin Heidelberg 2017

Abstract Tropical cyclones (TCs) are one of the most devastating natural phenomena. This study examines the capability of a global climate model with grid stretching (CAM-EULAG, hereafter CEU) in simulating the characteristics of TCs over the South West Indian Ocean (SWIO). In the study, CEU is applied with a variable increment global grid that has a fine horizontal grid resolution ($0.5^\circ \times 0.5^\circ$) over the SWIO and coarser resolution ($1^\circ \times 1^\circ$ — $2^\circ \times 2.25^\circ$) over the rest of the globe. The simulation is performed for the 11 years (1999–2010) and validated against the Joint Typhoon Warning Center (JTWC) best track data, global precipitation climatology project (GPCP) satellite data, and ERA-Interim (ERA-INT) reanalysis. CEU gives a realistic simulation of the SWIO climate and shows some skill in simulating the spatial distribution of TC genesis locations and tracks over the basin. However, there are some discrepancies between the observed and simulated climatic features over the Mozambique channel (MC). Over MC, CEU simulates a substantial cyclonic feature that produces a higher number of TC than observed. The dynamical structure and intensities of the CEU TCs compare well with observation, though the model struggles

to produce TCs with a deep pressure centre as low as the observed. The reanalysis has the same problem. The model captures the monthly variation of TC occurrence well but struggles to reproduce the interannual variation. The results of this study have application in improving and adopting CEU for seasonal forecasting over the SWIO.

1 Introduction

Tropical cyclones (TCs), one of the most devastating natural phenomena (Girishkumar and Ravichandran 2012), can be catastrophic to coastal communities. TCs and associated storm surges cause severe flooding, damage properties and claim lives (Badarinath et al. 2012). Between 1952 and 2007, 152 cyclones out of a total of 633 over the South West Indian Ocean (0° – 40° S; 30° – 75° E) made landfall in Madagascar and/or Mozambique (Mavume et al. 2009). For example, on February 22, 2007, TC Favio made landfall on the southern coast of Mozambique as a category 3 cyclone after developing in the South Indian Ocean a week earlier (Klinman and Reason 2008). Klinman and Reason (2008) also stated that Favio worsened an already occurring flooding situation and led to the deaths of 4 people and injured 70. Businesses, hospitals, schools and a prison (from which 600 inmates escaped) were destroyed. The flooding displaced over 120,000 people in Mozambique. More recently, on February 25 2013, TC Haruna pounded heavily on Madagascar. The country's National Disaster Risk Management Office reported that more than 17,000 people were affected by the storm with 13 reported deaths and 1500 homes flooded or destroyed (IRIN 2015). In light of devastating impacts of TCs, several TC modelling studies have been conducted in order to provide accurate early warning systems based on predictions of the behaviour of TCs

✉ Babatunde J. Abiodun
babiodun@csag.uct.ac.za

¹ Climate System and Analysis Group, Department of Environmental and Geographical Science, University of Cape Town, Cape Town, South Africa

² Teraflux Corporation, Boca Raton, FL, USA

³ Department of Oceanography, University of Cape Town, Cape Town, South Africa

⁴ South African Environmental Observation Network, Egagasini Node, Private Bag X2, Roggebaai, Cape Town 8012, South Africa

(Chatzidimitriou and Sutton 2005). Over the South West Indian Ocean (SWIO), these studies are vital for the vulnerable nations of Mozambique and Madagascar that face high risks of damage and loss of life from these systems (Klinman and Reason 2008). These two countries are amongst the developing countries of the world and their high vulnerability to TCs further compounds the socio-economic issue. Hence, there is a need for a more understanding of these systems.

Early modelling experiments have shown the applicability of Global Climate Models (hereafter GCMs) in simulating TCs (e.g. Manabe et al. 1970; Bengtsson et al. 1995, 1996; Vitart et al. 2003). However, most of them are based on the simulation of TC-like structures with low-resolution (more than 100 km) GCMs. Some of the characteristics of those low-resolution model cyclones, such as the spatial and temporal distribution, resemble, to a certain degree, observed TCs. The main limitation with these modeled cyclones is that the intensities of the simulated TCs are weaker and the spatial scales are larger than observed TCs due to the low resolution (Vitart et al. 1997). This limitation makes it difficult to simulate small-scale features, which are important to many physical processes such as rapid intensification of TCs. Bengtsson et al. (1995, 1996) performed a 5-year simulation with the European Centre Hamburg Model 3 (ECHAM3) at 100 km horizontal resolution and found that the model could simulate some aspects of the structure of TCs including spatial distribution and seasonal variability. They concluded that in certain areas, particularly in the northeast Pacific, a more realistic number of TCs was generated by the model only when the horizontal resolution was finer than 100 km. Regional Climate Models (RCMs) with a limited model domain can be run at higher resolutions than GCMs. However, they are compromised by the accuracy of boundary conditions. This can be especially problematic for TCs because they are often strongly influenced by large-scale systems that operate on spatial scales of thousands of kilometers (Gray 1979). A partial remedy for this boundary condition problem is to couple a RCM with a lower resolution GCM (e.g. Mbedzi 2010) in order to study large scale systems, but RCM boundary condition errors can lead to weak representation of large-scale processes like El Niño Southern Oscillation (ENSO) and Madden–Julian oscillation (MJO) that are known to drive TC activity (Strachan et al. 2013).

Attempts have been made to resolve low-resolution issues with GCMs by employing high resolution GCMs (Zhao et al. 2012; Strachan et al. 2013; Bell et al. 2014; Walsh et al. 2015). However, most of these use uniform resolution and require massive computing time and resources—a less than ideal match for the developing nations of the Southern African Development Community (SADC) due to financial and resource constraints.

Although variable-resolution GCMs have proven to be an invaluable tool in simulating TCs (e.g. Zarzycki et al. 2014; Harris et al. 2016; Hashimoto et al. 2016), not much has been done in utilizing these GCMs in studying TCs over the SWIO. Such an application is the focus of this study.

The Community Atmosphere Model with non-hydrostatic Euler-Lagrangian dynamical core (CAM-EULAG, hereafter CEU) has been shown to be more computationally economical and efficient as compared to GCMs with uniform high-resolution grids (Abiodun et al. 2008, 2011). Abiodun et al. (2008) conducted three aqua-planet simulations using CAM3 with each of the dynamical cores EULAG (CEU), finite volume (CFV) and Eulerian Spectral (CES). They found out that CEU adequately captured the result of CFV and CES and was therefore shown suitable for climate simulations. Abiodun et al. (2011) compared the simulated rainfall between CEU and CFV over West Africa during the boreal summer from 1996 to 2006 and found that CEU outperformed CFV even at the same uniform grid of $2^\circ \times 2.5^\circ$. Application of a stretched-grid improved results further. Ogier (2013) applied CEU to study the characteristics of inertial gravity waves over Southern Africa and observed that CEU showed that the interaction between horizontal wind and topography is an important cause of inertial gravity wave activity over southern Africa. Driver (2014) studied rainfall variability over southern Africa and found out that CEU captured some of the essential features of rainfall over southern Africa, such as the band of precipitation associated with the ITCZ as well the area of minimum rainfall over the South Atlantic Ocean. CEU has not yet been applied in the study of TCs. This study presents the first known application of CEU in simulating TCs.

The aim of the present study is to evaluate the performance of a GCM with grid stretching in simulating the characteristics of TCs over the SWIO ($0\text{--}40^\circ\text{S}$; $30\text{--}75^\circ\text{E}$) (Fig. 1). The evaluation focuses on the ability of CEU to simulate the climatology of the study area during the TC season (November–April), the structure and intensity of TCs, the interannual and seasonal variability of TCs, and TC genesis and tracks. Section 2 describes the observations, reanalysis and simulated datasets used in the study as well as the methods. The results of this study are discussed in Sect. 3 and conclusion in Sect. 4.

2 Data and methods

2.1 Data

We analysed observational, reanalysis, and model simulation data for the study period (1999–2010). The observational data includes the Joint Typhoon Warning Center (hereafter JTWC) best track data, obtained online at

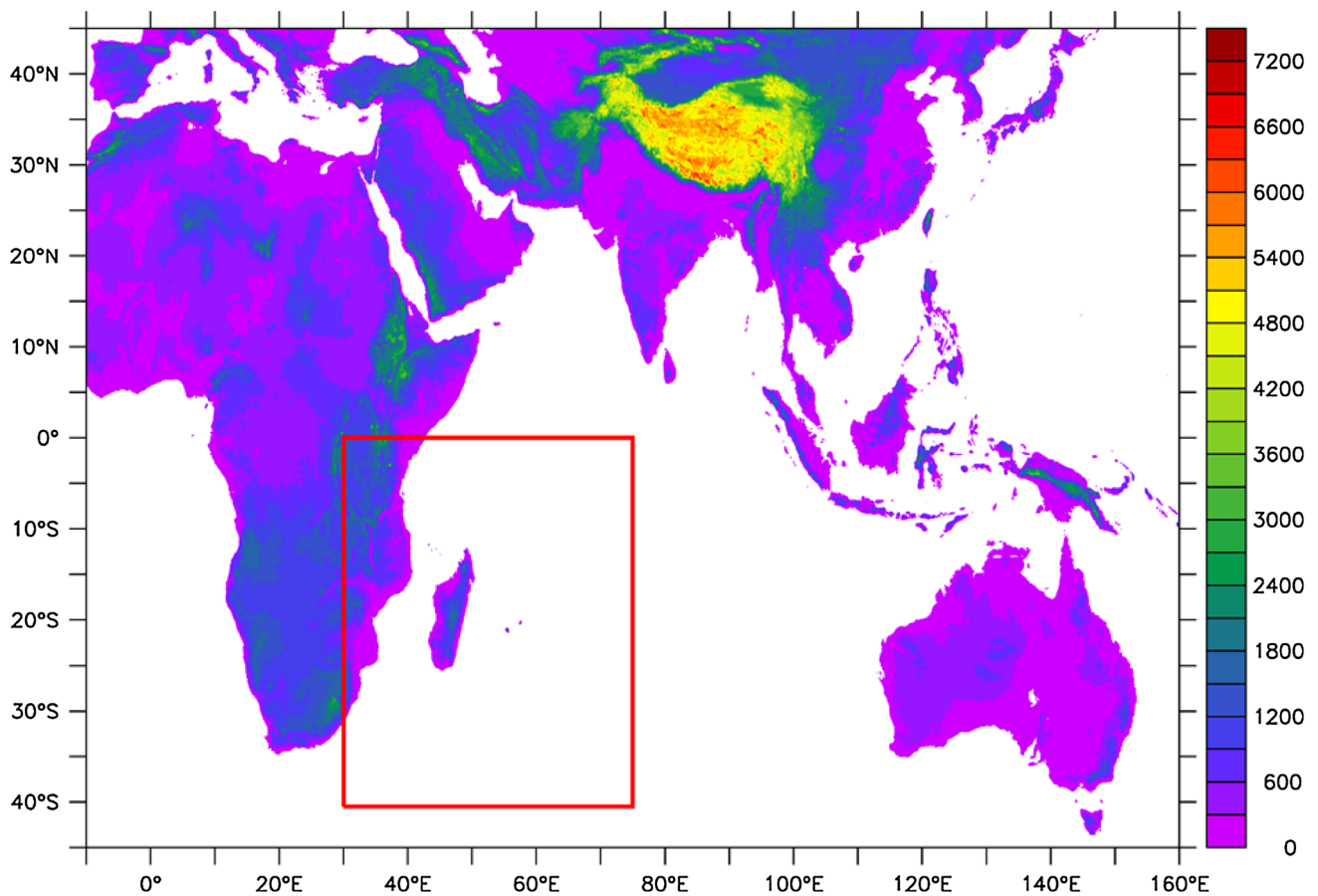


Fig. 1 Topographical map (in metres) showing the South West Indian Ocean basin defined by coordinates 0°–40°S; 30°E–75°E

<http://www.usno.navy.mil/JTWC>. Since the study period is from November 1999 to 2010, we elected to only use JTWC best track because there is not much difference between JTWC and the Regional Specialized Meteorological Centre La Réunion Dataset in the 2000s (Schreck et al. 2014). The JTWC uses the Dvorak technique (Dvorak 1984) to estimate TC intensity, which is based on the analysis of cloud patterns in visible and infrared satellite imagery. The best track data contains TC centre locations, the minimum surface level pressure (MSLP), and maximum surface wind (MSWs) at 6-hourly intervals and is used to validate CAM-EULAG (CEU) and ERA-Interim (ERAINT) with regards to the spatial patterns of TC tracks, genesis locations, intensities, as well as the variation of TCs on monthly and annual time scales. Monthly observed precipitation was obtained from the Global Precipitation Climatology Project Version 2.2 (hereafter GPCP) and is obtainable from <http://www.esrl.noaa.gov/ps>. The GPCP dataset, which combines global observation and satellite precipitation data at $2.5^\circ \times 2.5^\circ$ grid resolution, is used to evaluate the ERAINT and CEU simulated rainfall over the SWIO basin.

The monthly and 6-hourly reanalysis precipitation, wind, vorticity, vertical velocity and temperature data, with a spatial resolution of 80 km (T255 spectral) and 60 vertical levels, were obtained from the ERA-Interim (ERAINT) dataset <http://www.ecmwf.int/en/research/climate-reanalysis/era-interim> and compared with CEU simulations over SWIO during TC season (November–April). More information about ERAINT can be found in Berrisford et al. (2011).

2.2 Model description and experiment

CEU is a non-hydrostatic global climate model with grid stretching capabilities (Abiodun et al. 2008). It uses the Community Atmosphere Model Version 3 (hereafter CAM3) physics routines and Euler-Lagrangian (EULAG) dynamics. CAM3 is the fifth generation of the atmospheric model component of the Community Climate System Model (CCSM), which also includes land, ocean and thermodynamic sea-ice components. A complete description of CAM3 can be found in Collins et al. (2004). The physics package consists of moist processes, cloud and

radiation calculations, surface models and turbulent mixing processes. A particular feature of CAM3 is the use of a microphysical parameterization scheme that is similar to cloud resolving models. However, higher grid resolution simulations (~ 20 km) are required in order to take advantage of these advances than what the standard CAM3 offers (~ 200 km). CAM3 has a clean separation between the dynamics and physics parameterizations, which allows for relatively easier replacement of either set of subroutines. This separation allows for the replacement of the dynamical core by EULAG, a non-hydrostatic, parallel computational model for all-scale geophysical flows. The non-hydrostatic behaviour of EULAG is achieved through the anelastic approximation of the equations of motion which are solved in a EULERian (flux form) or a LAGRangian (advective form) framework. EULAG combines non-oscillatory forward-in-time (NFT) numerical algorithms with a robust elliptic Krylov solver. The key signature of EULAG is that it is formulated in generalized coordinates that enable grid

adaptivity. These features give EULAG a novel advantage over the existing dynamical cores in CAM3 (Abiodun et al. 2008).

In the present study, the CEU grid is stretched to a resolution of $0.5^\circ \times 0.5^\circ$ (meridional \times zonal) over the SWIO, $1^\circ \times 1^\circ$ over much of the globe and $2^\circ \times 2.5^\circ$ over the Pacific Ocean and poles (see Fig. 2). The stretching factor was 4.5 along the longitude and 1.5 in the latitudinal direction, which satisfies the Caian-Geleyn condition of limiting the stretching factor to values less than 8 in order to minimize pole-symmetric dilations (Caian and Geleyn 1997). The prevailing advantage of using a stretched grid is the ability to apply higher resolution over an area of interest in a global model without needing as substantial an increase in computational power as required by a uniform high resolution grid. Using scaling results from idealized dry global simulations, we estimate that the 50 km stretched grid uses about 1/8 of the CPU time required by a 50 km uniform high-resolution global grid. The model simulation uses 26

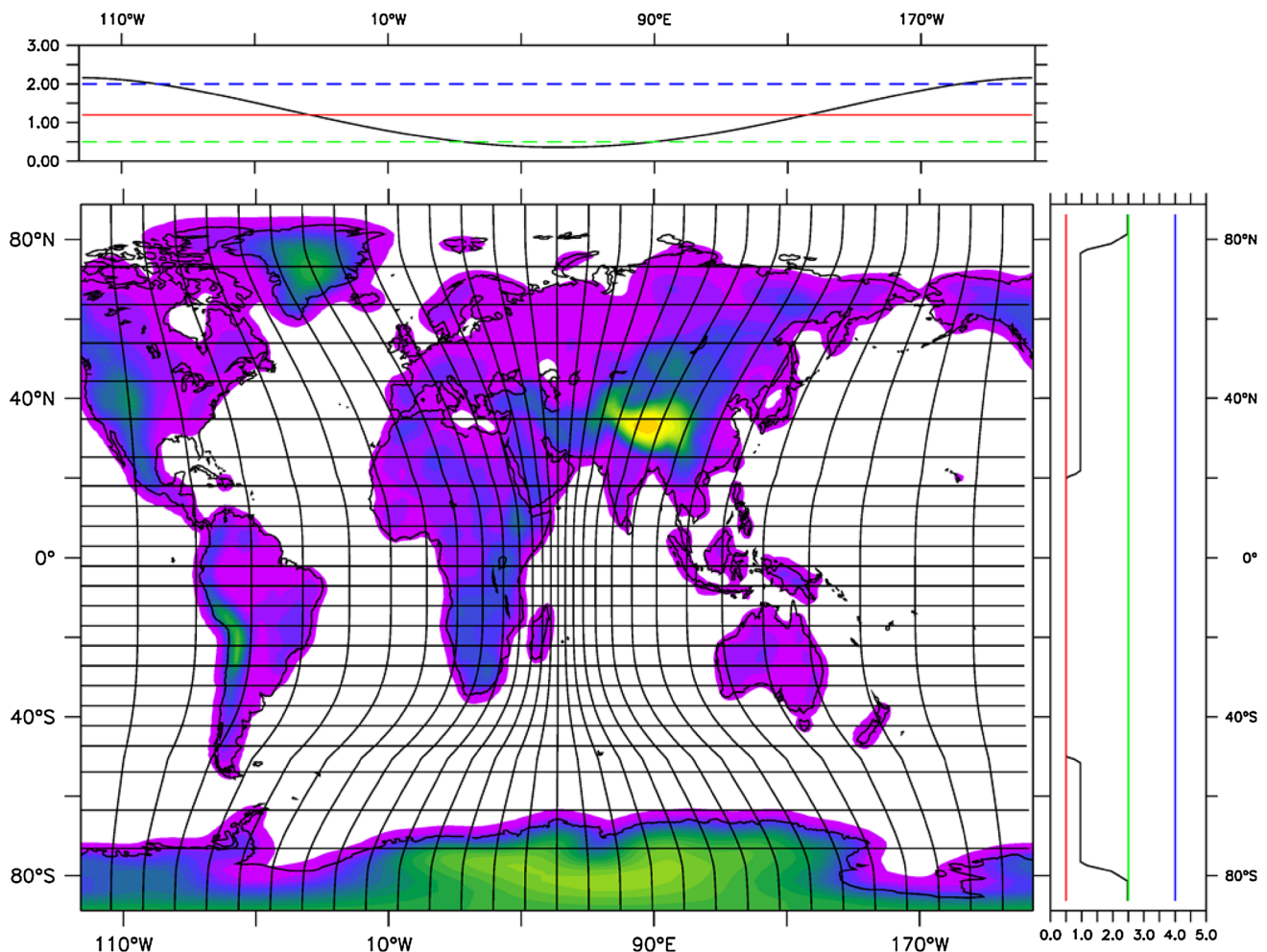


Fig. 2 The CAM-EULAG model stretch grid setup with the highest resolution ($0.5^\circ \times 0.5^\circ$) over the South West Indian Ocean (0° – 40° S; 30° – 75° E). The *top* and *right panels* show the scaling zonal and meridional resolutions, respectively

vertical levels with an integration time step of 30 s (i.e. dynamic time step) and a sample output rate of 6-hourly data. The physics routines have different time step; it is about 30 s for the boundary layer schemes and 360 s for the radiation scheme. The simulation was forced with observed sea surface temperature (SST) data (obtained from the Hadley Centre) and the Community Land Model (CLM, version 2.1) was used in the simulation. The model topography was obtained by interpolating the CLM dataset into the CEU stretched grid (shown in Fig. 2).

CEU did not scale well on our computing system. For the model set-up used in this study, the model scalability dropped fast after 64 processors such that it did not make sense to use more than 64 processors for the simulation, even though we had access to about 400 processors. With 64 processors, it took the model about 3 months to complete a 1-year simulation, meaning that a continuous 11-year run was going to take 33 months (2 years, 9 months!). Given the limited computing time available for the study, it was not feasible to embark on a continuous the 11-year simulation. Hence, to create a climatology for the SWIO TC season, 11 simulations of 1-year run were performed in parallel. That reduced the simulation period to about 6 months. Each run started (at rest) from August of the previous year until July of the years from 1999 to 2010. Abiodun et al. (2008) showed that CEU reached statistical stationarity in approximately 40 days by looking at the time evolution of the zonal average of (a) zonal wind, (b) potential temperature and (c) specific humidity in an aqua-planet simulation. In addition, Driver (2014) showed a similar spin-up time (40 days) when CEU was initialised with more realistic atmospheric conditions. Therefore, the first 3 months were discarded as spin-up (i.e. August, September, and October). The SWIO TC season months (November–April) were used for all the following analyses and discussions.

2.3 Methods

In this study, TCs are defined as any warm core, non-frontal, low pressure systems that develop over tropical or subtropical waters with a closed cyclonic surface circulation about a well-defined centre with 10 m winds greater than 17 m s^{-1} . Storms that are identified as extratropical are excluded from the data used here since this study focuses purely on storms identified as TCs (Holland 1993).

2.3.1 Tropical cyclone detection and tracking algorithm

An objective procedure for detecting and tracking TCs in this study uses a similar method to that described by Vitart et al. (1997), Kleppek et al. (2008) and Zarzycki

and Jablonowski (2014). The TCs were detected in 6-hourly ERAINT and CEU output as follows:

- The centre of a low-pressure system was detected by finding a closed minimum MSLP around an 8×8 grid. For each low-pressure system, the nearest minimum vorticity smaller than $-3.5 \times 10^{-5} \text{ s}^{-1}$ was detected. This minimum must occur within 4° of the centre of the low-pressure system.
- The closest local maximum of 850–300 hPa average temperature is defined as the centre of the warm core. The average temperature must be greater than 0°C . The warm core is defined within 2° from the centre of the low pressure.
- The wind speed at 10 m is used as recommended by Walsh et al. (2007) during the detection phase. The maximum wind speed within 5° of the storms centre must be greater than 17.00 m s^{-1} .

Once a candidate TC has been detected:

- Search for the nearest storm within 500 km following the 6-hour period. If a storm is detected, it is considered to be the same storm. However, if there is no storm, then the track of the storm is considered to have stopped.
- The storm must persist for at least 2 days to be considered a TC (Zarzycki and Jablonowski 2014)

2.3.2 Performance Measures

The interannual variability of the observed, reanalysis and simulated TC anomaly patterns were computed using phase synchronisation (η) that quantifies how well the model simulates or captures the timing of patterns. This is defined by Misra (1991) as:

$$\eta = \left(\frac{n'}{n} \right) \times 100$$

where n' is defined as the number of years in which the simulations are in phase with the observation (i.e. both observed and simulated annual TC count anomalies are simultaneously positive or negative), while n is the total number of years in the study (11 years). The phase synchronisation η will be 0% (i.e. no synchronisation) if all the simulated TC occurrence anomalies are out of phase with the observations, or 100% if all the simulations are in phase (i.e. perfect synchronisation). Several studies (e.g. Araujo et al. 2014; Tozuka et al. 2014) have used synchronisation to evaluate the accuracy of phase differences between model and observed datasets.

The accumulated cyclone energy (ACE) is used to calculate the interannual variability of TC activity over the SWIO. ACE is an integrated measure of TC activity which combines intensity and duration (Bell et al. 2000). ACE is defined as:

$$\text{ACE} = 10^{-4} \sum v_{\max}^2$$

where v_{\max} is the MSW (maximum surface wind in knots) for a TC at a given time. The sum is taken over all 6-hourly time-steps during a TC's lifetime. ACE from individual TCs can be summed regionally in order to produce basin-wide statistics.

The pressure-wind relationship was used to highlight the ability of the model in producing the correct surface gradient wind balance for a given sea level pressure deficit.

The non-parametric Spearman rank correlation was used to calculate the correlation of ERAINT and CEU with respect to observation on the inter-annual variability of TC occurrence. Spearman's rank correlation was chosen since it does not assume that dataset is described by a normal distribution. Furthermore, Spearman's rank correlation overcomes the effect of outliers and skewness by considering the rank values of the data instead of the magnitude. The rank correlation is defined as:

$$\rho = 1 - \frac{6 \sum d_i^2}{n(n^2 - 1)}$$

where n is the sample size which is calculated by years in each dataset (i.e. the sample size is 11 for CEU, ERAINT and JTWC) and d_i is the difference between the rank of corresponding values of two datasets.

3 Results and discussion

3.1 Climatology of tropical cyclones over the South West Indian Ocean

Although previous studies have established the capability of CEU in simulating the climate over various regions (Abiodun et al. 2011; Ogier 2013; Driver 2014), none of them evaluated the model over the SWIO region. Therefore we begin the study by comparing the regional climate produced by CEU over the SWIO with GPCP and ERAINT. The validation focuses on how well CEU simulates the temporal and spatial variation of essential climatic features in rainfall and vorticity during the TC season (November–April).

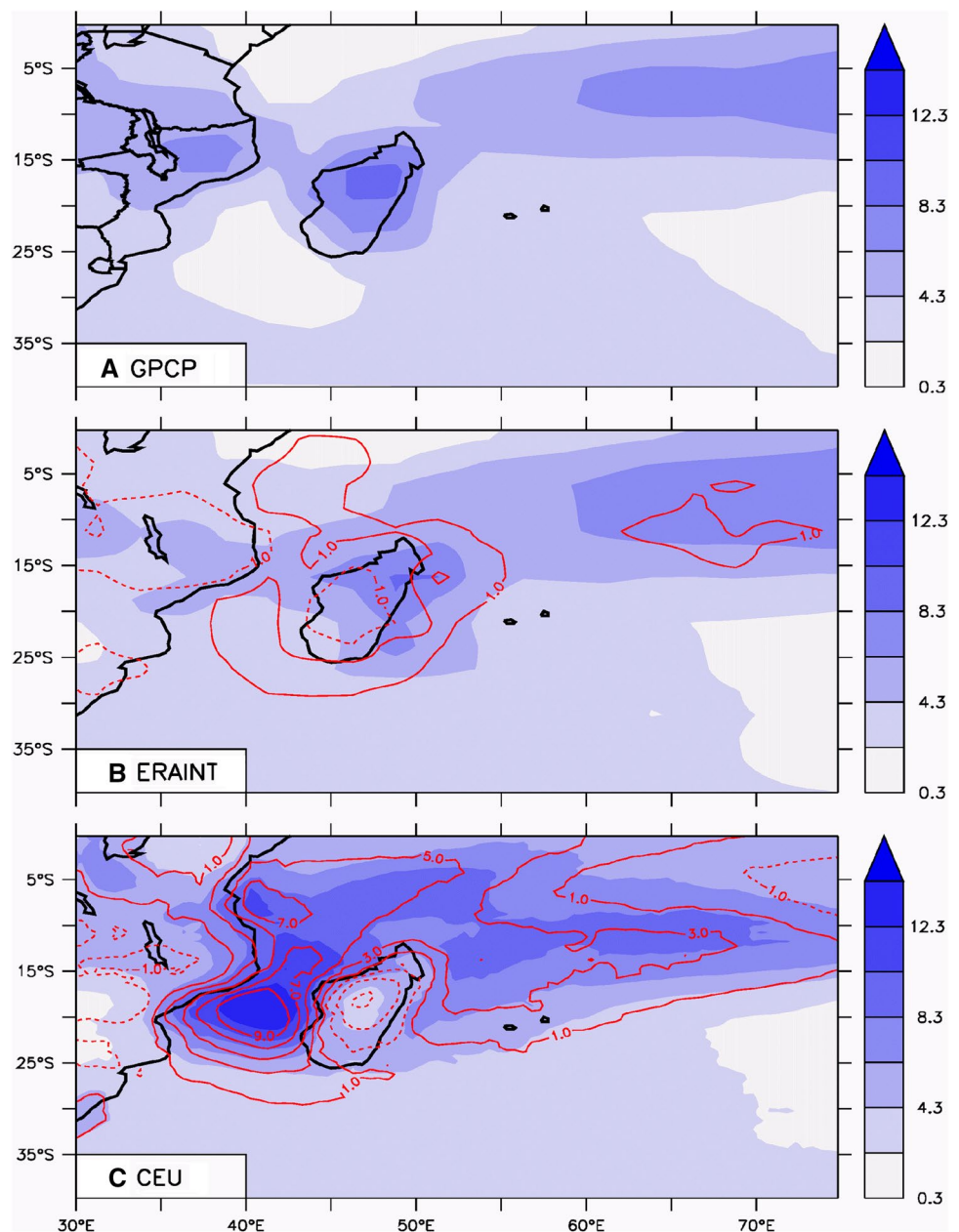
3.1.1 Rainfall

There are common features in the rainfall distributions produced by the CEU simulation, ERAINT, and GPCP observation over the SWIO (Fig. 3). GPCP shows a band of maximum rainfall (associated with the Inter Tropical Convergence Zone, ITCZ) around 5–20°S and an area of minimum rainfall over the Mozambique Channel (around 35–45°E; 20–35°S) (Fig. 3a). The GPCP rainfall band shows a local maximum over Mozambique (about 8 mm day⁻¹) and over Madagascar (about 12 mm day⁻¹). ERAINT reproduces well the rainfall band but fails to capture the local maximum over Mozambique. In addition, ERAINT does not reproduce the minimum rainfall over the Mozambique Channel (MC) as in GPCP, while CEU simulates a local maximum over the area. The rainfall bias over the MC is within ±1 mm day⁻¹ in ERAINT but up to 9 mm day⁻¹ in CEU. The wet bias could be due to the convective parameterization in the model; the parameterization may be too sensitive to the warm boundary layer over this area. It could also be due to a more generic resolution sensitivity of moist physics. This has been highlighted for older CAM physics by Williamson (2008). However, the overestimation of the deep convection in this area may be responsible for the inability of CEU to simulate the local maximum rainfall over the Madagascar area, because local areas of deep convection can suppress convection in adjacent regions, leading to the lack of a rainfall maximum. The CEU dry bias over Madagascar is consistent with the warm bias over the area (figure not shown), because less rainfall results in reduced cloud albedo, more incoming solar radiation, and more heat.

3.1.2 Vorticity

The CEU simulated 850 hPa vorticity field has common features with those in ERAINT results (Fig. 4). ERAINT shows a large area of negative vorticity approximately 50–75°E; 0–20°S, which is consistent with the ITCZ since negative vorticity values in the southern hemisphere lead to surface convergence. Moreover, this result is consistent with the observed GPCP precipitation (Fig. 3a) since areas of high surface convergence are favourable to the formation of convective precipitation. Below 25°S, ERAINT shows positive vorticity values which are associated with the South Indian high pressure system. Moreover, positive vorticity values associated with the South Indian High Pressure System indicate areas of subsidence where convective rainfall is often inhibited. Therefore, this result further highlights the difference in rainfall patterns between areas in the vicinity of the ITCZ and South Indian high pressure system. CEU is in agreement with ERAINT with regards to the spatial pattern of the ITCZ as well as areas

Fig. 3 Climatological rainfall over the South West Indian Ocean for TC season November–April 1999–2010 in mm/day. The *red contours* in **b** and **c** show the bias between the ERAINT and CEU rainfall with respect to GPCP i.e. CEU-GPCP and ERAINT-GPCP. *Solid contours* denote a wet bias and *dashed contours* indicate a dry bias



of subsidence. However, the CEU vorticity field over the MC is much stronger than the reanalysis. This strong bias is consistent with the models wet bias over that region.

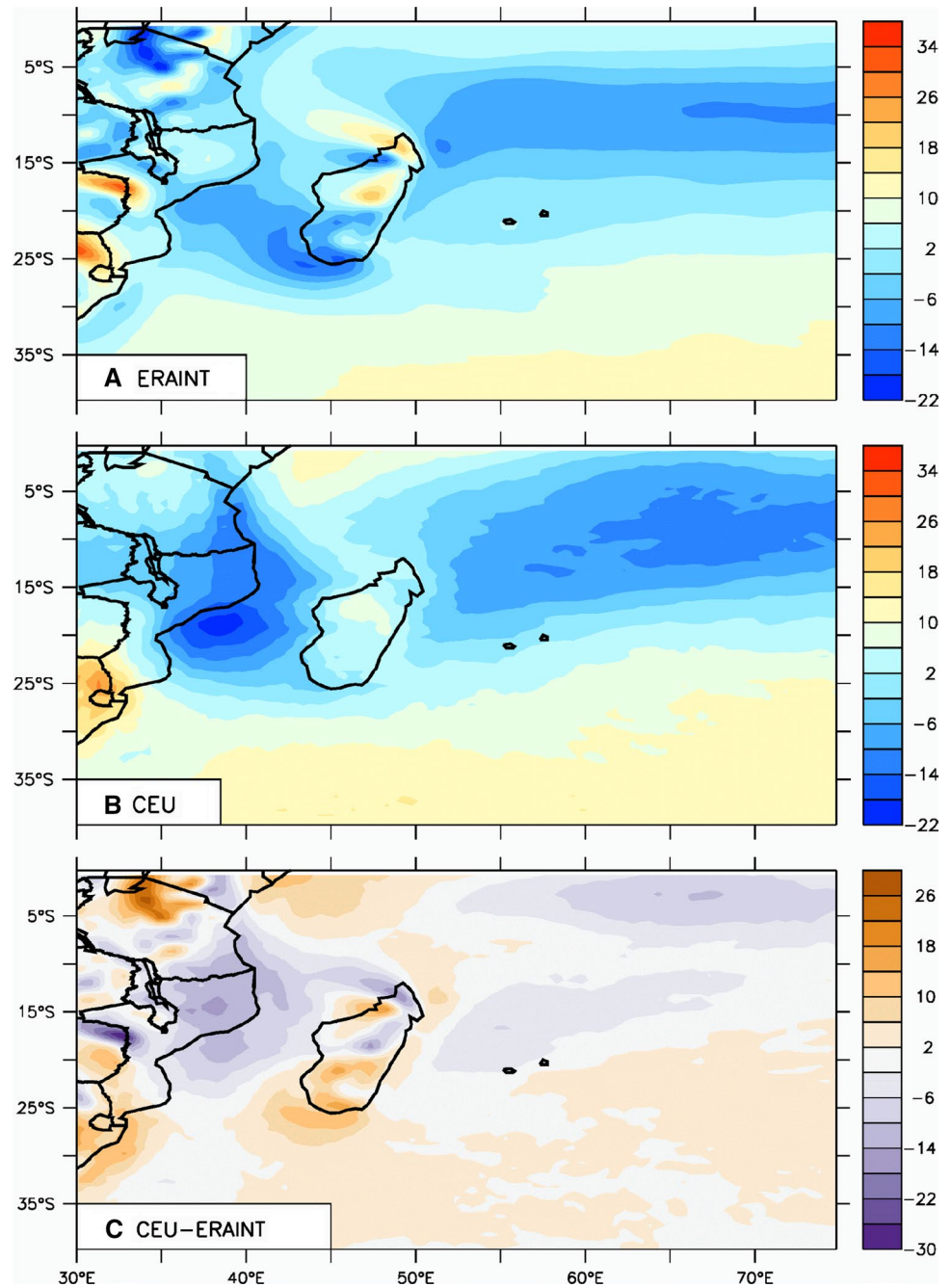
3.2 Simulated tropical cyclone structure

Figures 5 and 6 show details of TC storm structure from ERAINT and CEU, respectively. Since ERAINT is reanalysis, it is able to simulate actual storms in the JTWC dataset and in fact the TC depicted in Fig. 5 is TC Hary 2002. CEU on the other hand develops its own realization of climate and does not show close correspondence with any particular JTWC TC during the 11 year period. For comparative

purposes we have selected a TC out of the CEU dataset that is similar to ERAINT's TC Hary 2002 in duration, size, and intensity. This is the storm depicted in Fig. 6.

ERAINT TC Hary 2002 (Fig. 5) formed in the SWIO on the 7th of March 2002 as a tropical depression (minimum MSLP of 1007 hPa) reaching MSWs of 36 ms^{-1} on the 10th of March when it brushed the north eastern parts of Madagascar. It reached a wind intensity of 29 ms^{-1} (minimum MSLP of 973 hPa) on 11 March 2002 and transitioned into an extra-tropical cyclone on the 17th of March. JTWC data indicate TC Hary formed on March 5 2002 and dissipated on March 17 2002. Figure 7 shows the ERAINT TC Hary (red) has a very similar track to the observed JTWC TC

Fig. 4 850 hPa climatological vorticity over the South West Indian Ocean for TC season November–April 1999–2010 in 10^{-6}s^{-1} . **c** shows the difference between CEU and ERAINT



Hary (blue). Overall, the timing of TC development and trajectory match the observations very well. The quality of the ERAINT trajectory verifies the ability of the objective TC detection algorithm in tracking TCs in gridded datasets. Note however that the maximum surface wind of ERAINT Hary is about half of the JTWC observed value of 72 ms^{-1} .

Figure 6 shows the comparable CEU TC. This storm appeared on the 21st of January 2000 in the SWIO as a tropical depression with a maximum 850 hPa wind intensity of 26 ms^{-1} . It strengthened into a TC, reaching a maximum surface wind intensity of 39 ms^{-1} (minimum MSLP

of 973 hPa) on the 23rd of January 2000. The 10 m horizontal wind at the storm's peak is shown in Fig. 6a. Similar to ERAINT (Fig. 5a), the CEU TC exhibits a calm eye and strong cyclonic winds surrounding the eye (Fig. 6a). In both results, the highest wind speeds occur on the left side relative to the storm motion (Figs. 5a, 6a) which is a common feature of southern hemisphere TCs. Note some spiral band structure appears north and southwest of the CEU storm core (Fig. 6a), a feature that does not appear in the ERAINT TC (Fig. 5a). Figures 5b and 6b show the warm cores that are associated with diabatic heat release in

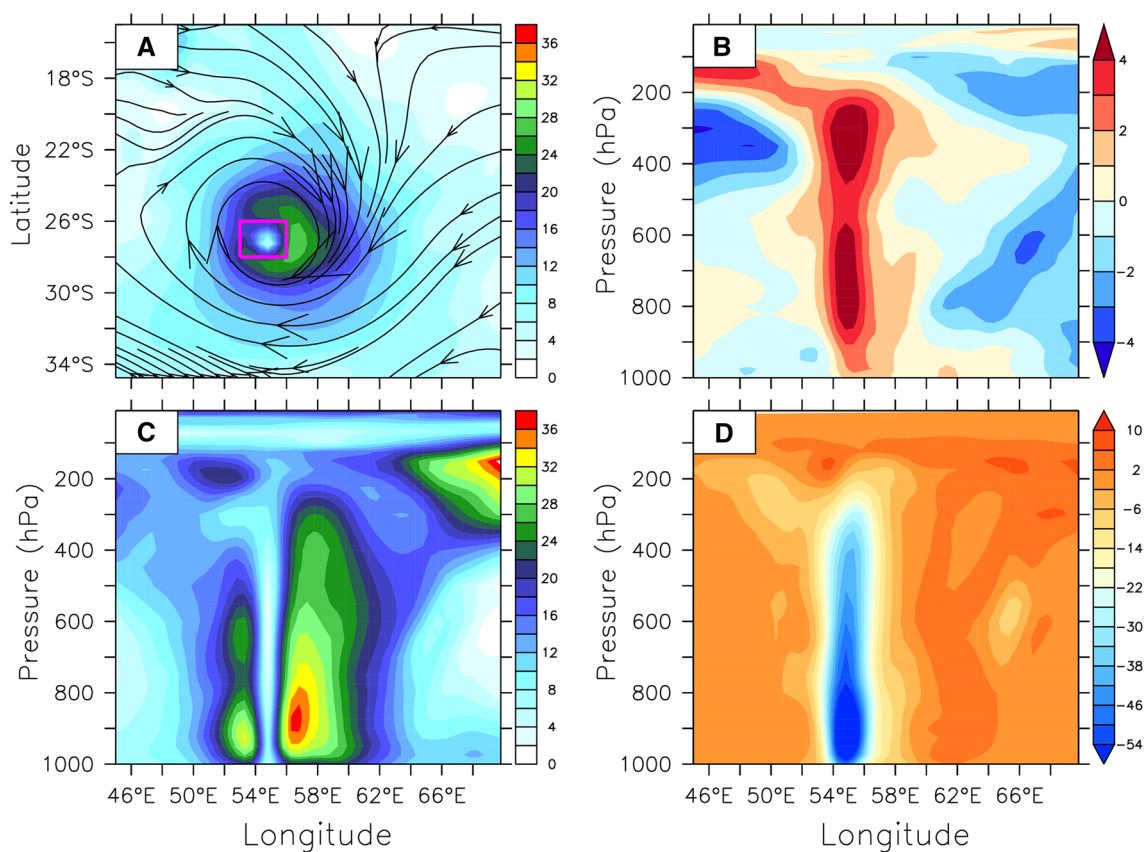


Fig. 5 Dynamical structure of a mature stage TC as simulated by ERAINT on the 11th March 2002. **a** The 10 m horizontal wind distribution in m s^{-1} , **b** The warm core in $^{\circ}\text{C}$, **c**, **d** the vertical cross-section of the wind speed (in m s^{-1}) and vorticity (in 10^{-5} s^{-1}) respectively

the two TCs. The cores are seen to extend from 950 to 150 and 900–200 hPa in ERAINT and CEU, respectively. For CEU, the TC detection algorithm (see Sect. 3.3.1) indicates an average temperature excess of 6° from 850 to 300 hPa. The ERAINT warm core is stronger and deeper. These difference trends are mirrored in the vertical wind fields (Figs. 5c, 6d) and vorticity (Figs. 5d, 6d). Maximum wind speeds are similarly confined to lower levels (Figs. 5c, 6c). The eyewall diameter is very similar between the 2 results; both have eyewall diameter $\sim 1^{\circ}$ at lower levels that slowly increases to $\sim 2^{\circ}$ at upper levels (Figs. 5c, 6c). Both CEU and ERAINT simulate well the relative vorticity in the centre of the storm with the largest values of negative relative vorticity in the lower levels (Figs. 5d, 6d). The negative low-level vorticity represents the spinning of a cyclonic rotating storm in the Southern Hemisphere.

Overall, the reanalysis storm is stronger and deeper, yet has a less detailed wind field than the CEU storm. These differences are likely due to a number of factors. First is the lower horizontal but greater vertical resolution and atmospheric depth of ERAINT vs. CEU. A second possible factor is that the numerical schemes of CEU's dynamical core are less diffusive at small scales as well as generate better

dynamical upscale transfers—allowing more realistic physics at a given grid resolution (Prusa and Gutowski 2010). Structural differences could also result due to the differing physical parameterization schemes employed. Last, sampling issues can affect the comparison. In particular, the ERAINT and CEU TCs are intrinsically different storms.

3.3 Simulated tropical cyclone intensity

3.3.1 Accumulated cyclone energy

Figure 8 shows the accumulated cyclone energy (ACE) for the JTWC data, reanalysis, and model. ERAINT correlates (spearman) much better with the observations ($\rho = 0.75$; p value = 0.01) in comparison to CEU ($\rho = -0.57$; p value = 0.07) on the interannual variability of ACE. The use of the observed atmospheric state in the reanalysis is obviously a significant factor in this comparison. Additionally, the poor CEU correlation may be due to the relatively short 11-year simulation and one model realization of ACE which could lead to lower correlation due to the presence of noise. Ensemble runs may improve the results (Goerrs 2000; LaRow et al. 2008; Hamill et al. 2011). The observed

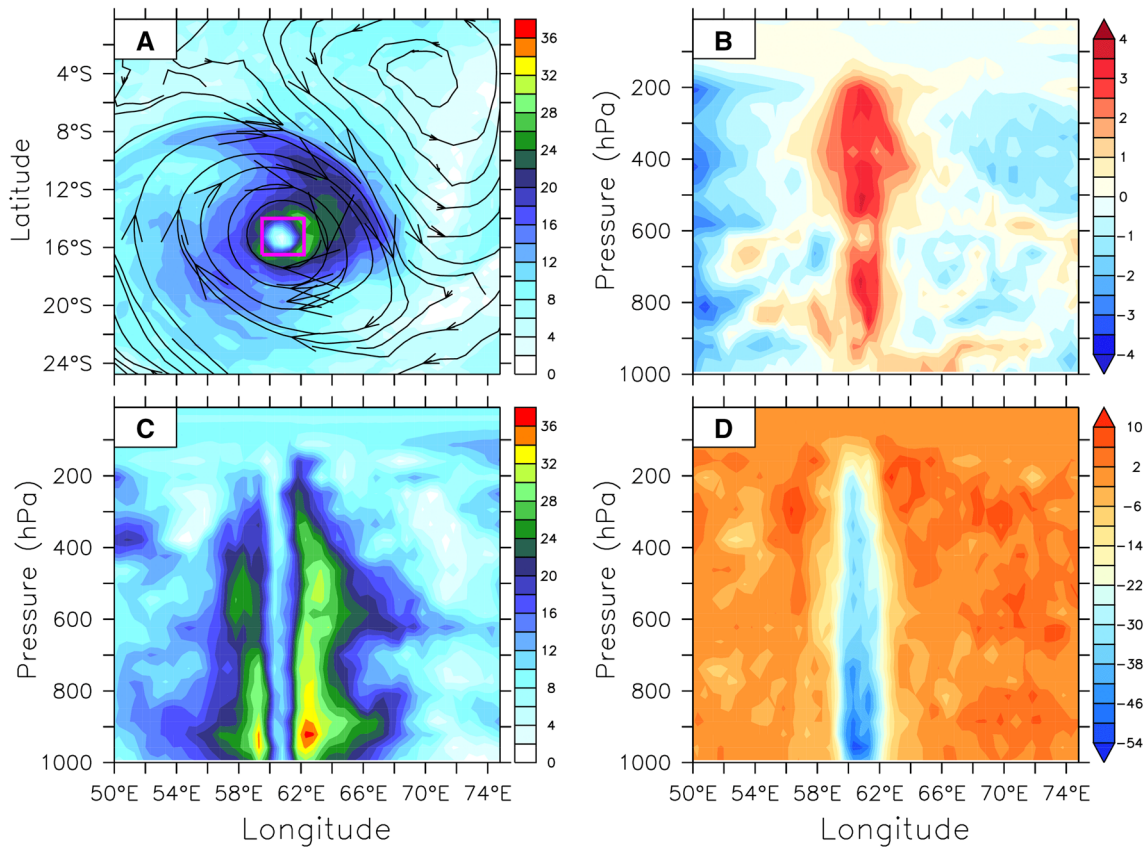


Fig. 6 Dynamical structure of a mature stage TC as simulated by CEU on the 23th January 2000. **a** The 10 m horizontal wind distribution in m s^{-1} , **b** the warm core in $^{\circ}\text{C}$, **c**, **d** the vertical cross-section of the wind speed (in m s^{-1}) and vorticity (in 10^{-5} s^{-1}) respectively

annual mean ACE over the SWIO basin is $138.31 \times 10^4 \text{ kn}^2$. By contrast, ERAINT and CEU show annual mean ACE of 39.28 and $62.06 \times 10^4 \text{ kn}^2$, respectively (Fig. 8). Although CEU does a much better job than ERAINT on the annual

mean ACE over the basin, it is still well below the JTWC observations. The factor of 2 differences in ACE values between ERAINT and CEU scales well with the effective grid resolution ratio of the models, suggesting these discrepancies are largely due to insufficient grid resolution. Other issues, such as simulation noise noted above, may also be involved.

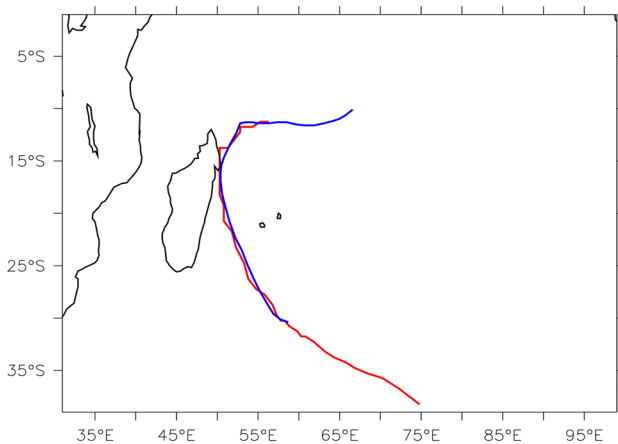


Fig. 7 Observed JTWC (blue) and ERAINT (red) Tracks for TC Hary which developed on the 5th of March 2002 over the South West Indian Ocean

3.3.2 Wind-pressure relationship

There is good overall agreement between observation, ERAINT and CEU on the wind-pressure relationship MSW (MSLP) shown in Fig. 9. Both CEU and ERAINT show the highest wind speeds corresponding with the lowest minimum MSLP, which is consistent with JTWC. The wind-pressure relationships were curve fit with a quadratic equation (lines shown in Fig. 9). The R^2 value of the JTWC data is 0.99 while ERAINT and CEU yielded R^2 values of 0.64 and 0.72 respectively—showing adequate skill in the gridded datasets. However, both the model and reanalysis fail to adequately produce the lower MSLPs seen in the observations, which drop to $\sim 900 \text{ hPa}$. Although both CEU and ERAINT have similar upper bounds as JTWC observations

Fig. 8 Interannual variability of the accumulated cyclone energy for observed (JTWC), ERAINT and CEU Tropical cyclones over the South West Indian Ocean

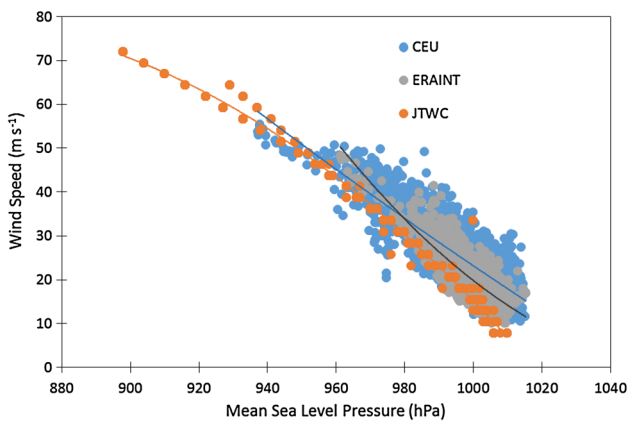
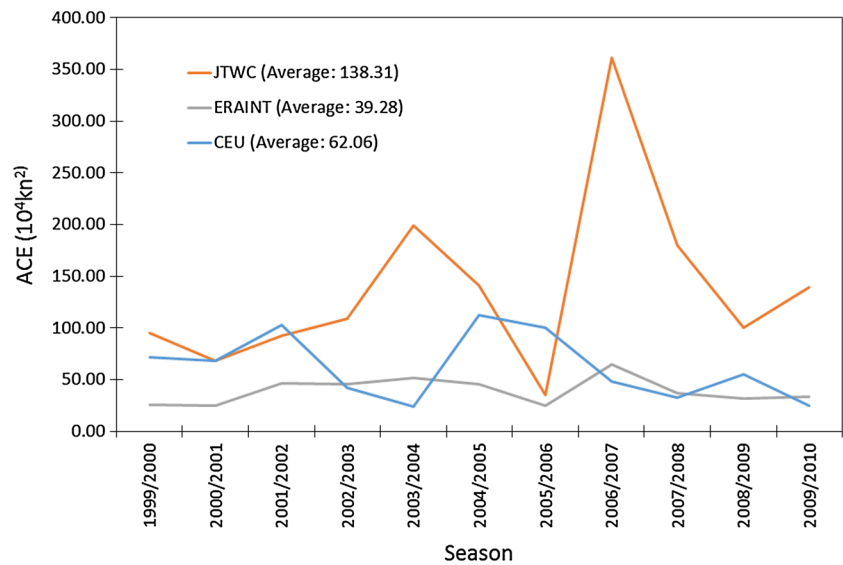


Fig. 9 Wind-pressure relationship of observed (JTWC), ERAINT and CEU TCs over the South West Indian ocean for November to April, 1999–2010

for MSLP ~1010 hPa, the lower bound for MSLPs is ~930 hPa for CEU vs. ~960 hPa for ERAINT. This strongly suggests grid resolution limitations. Hence, reanalyses (and likely CEU) are of insufficient resolution to fully capture the intense tail of the TC distribution [e.g., Schenkel and Hart (2012)].

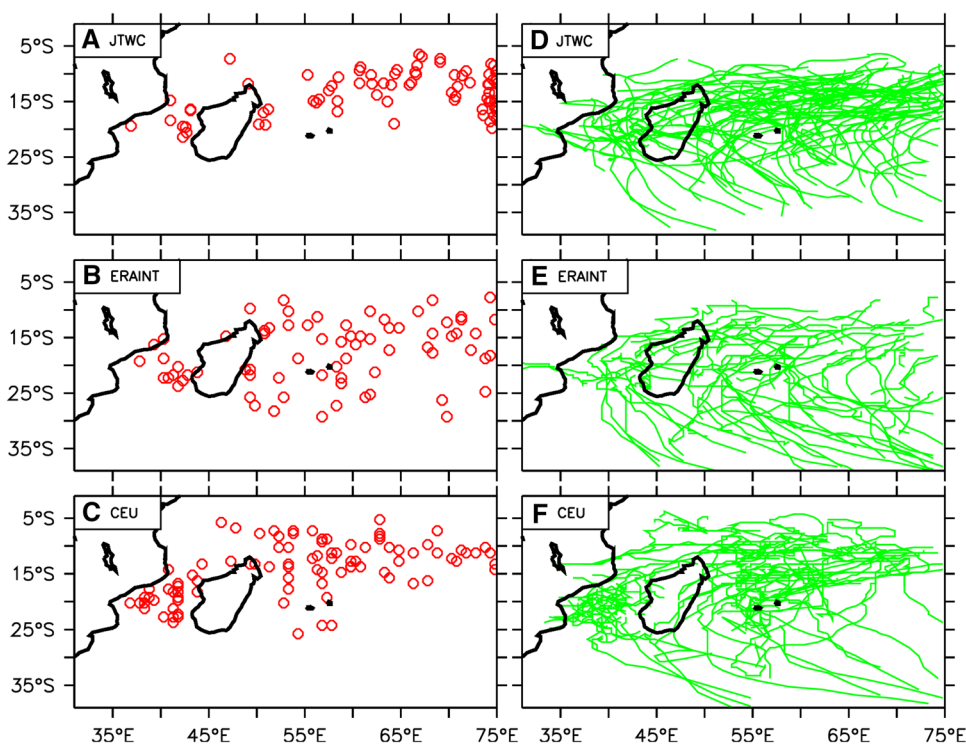
3.4 Spatial patterns of tropical cyclone tracks and genesis locations

Figure 10 shows TC genesis locations (right) and tracks (left) over the SWIO basin (0–40S°; 30–75E). Approximately 55% of all JTWC SWIO TCs formed in the eastern (65–75E) portion of the basin and moved westward with the aid of the south-east trade winds (zonal steering flow in Vitart et al. 2003); this pattern is similar to the findings

of Mavume et al. (2009). ERAINT had similar results with 51% of cyclogenesis events in the furthest east region. CEU had only 16% of TCs forming in the same region. This lack of cyclogenesis between 65°E and 75°E in CEU might be attributed to the lower resolution (>50 km) stretched area towards the edge of the basin. Approximately 28% of all CEU TCs formed over the MC compared to only 11% in the observation. This finding suggests that there is a strong TC bias present in CEU over the MC. Figure 4B strongly suggests that the 850 hPa vorticity anomaly present in CEU may be the chief cause of the substantial TC genesis over the MC since large values of vorticity aid in the formation of TCs (Gray 1968; Henderson-Sellers et al. 1998). By contrast, CEU does exhibit skill in the latitudinal distribution of genesis locations. For example, the TC genesis is mostly concentrated between 5° and 25°S and no TCs originate below 30°S, which is in agreement with observations. Furthermore, CEU agrees with the observation and ERAINT with regards to the lack of TCs forming close to the equator. Near the equator, the Coriolis parameter tends to zero and the development of strong organized vortices is generally inhibited.

As noted earlier, CEU simulations cannot be expected to match particular best fit trajectories of JTWC because it develops its own atmospheric synoptic flow details and TCs are exquisitely sensitive to those details. Yet it does generate plausible climate statistics. In particular, there is reasonable agreement between the observation (Fig. 10d), reanalysis (Fig. 10e) and model (Fig. 10f) on the spatial characteristics of TC tracks over the SWIO. The observation shows the largest concentration of TC activity approximately between 10–30°S and no TC activity near the equator. This result is consistent with earlier studies by Vitart et al. (2003) and Mavume et al. (2009). Near the Horse

Fig. 10 TC genesis locations (red dots) and tracks (green lines) over the South West Indian Ocean for TC seasons (November–April) from 1999 to 2010 for (a, d) JTWC best track data (observation), (b, e) ERAINT and (c, f) CEU



latitudes (30–35°S), observed TCs tend to recurve eastward due to the prevailing westerlies which are characteristic of the mid-latitude atmospheric circulation. Both ERAINT and CEU capture the spatial pattern of TC tracks very well. The reanalysis and model both show landfalling TCs over Madagascar as well as over the eastern parts of Mozambique. The most significant difference in the CEU tracks is a concentration of TC activity over the Mozambique Channel. Again, this can be attributed to the anomalous 850 hPa vorticity over the area (Fig. 4b). Last we note that CEU’s enhanced TC count over the MC may artificially increase the ACE over the basin since there are more TCs forming in comparison to the JTWC observations.

3.5 Monthly variation of tropical cyclone occurrence

CEU captures the basic monthly variation of the observed TCs over the SWIO (Fig. 11). It agrees with observations by showing peak TC activity in January and February—the peak of summer in the southern hemisphere when SSTs are high and the formation of TCs is favored. However, both the model and ERAINT overestimate the number of TCs for each of the two peak months (January and February) in comparison to the observation.

Out of the total CEU TCs that formed over the channel (i.e. 26), 14 (54%) formed in January, 8 (~31%) in February and 4 in other months. This firmly suggests that the MC bias in CEU is strongly exhibited in January and February when it shows a prevalence of TC genesis. Out

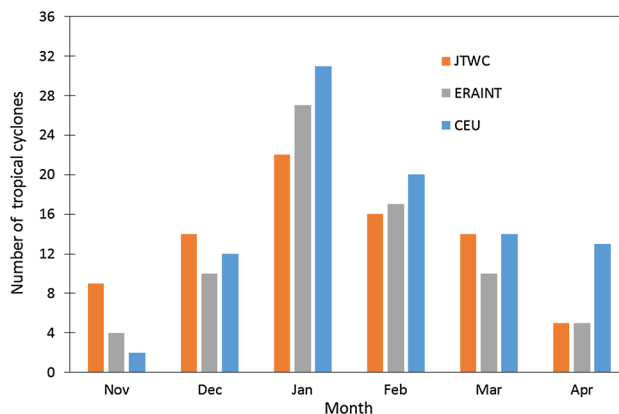


Fig. 11 Monthly variability of TCs over the South West Indian ocean for study period 1999–2010

of the 9 JTWC TCs that formed in the MC (Fig. 10a), 2 (22%) formed in January and February which is inconsistent with previous studies (e.g. Mavume et al. 2009). The inconsistency may be due to the time period of the 11 years which is too short to have robust statistics of the variability of MC TCs, Mavume et al. (2009) analysed TC data for 27 years (1980–2007) and showed 60% MC TCs forming in January and February. The model shows some skill in simulating TC numbers during December and March with marginal differences in comparison to the observation but struggles to adequately simulate TC counts for November and April.

3.6 Interannual variability of tropical cyclones

In the SWIO, TCs show variability on an annual basis with an average of 7.3 ± 2.2 observed JTWC TCs occurring per season. Climate variability modes (teleconnections) such as El Niño Southern Oscillation (ENSO), Indian Ocean Dipole (IOD) and South Atlantic Subtropical Dipole (SASD) are known to directly or indirectly impact TC activity in various ocean basins (Camargo and Sobel 2005; Saha and Wasimi 2013; Rodrigues et al. 2015). These three teleconnections in particular are relevant to the SWIO basin. ENSO is one of the most important coupled ocean–atmosphere teleconnections affecting interannual climate variability, while the IOD plays an important role in the interannual climate variability in the Indian Ocean (Saji et al. 1999). The SASD has an important role over the South Indian Ocean in strengthening the South Indian Ocean High Pressure system (also known as the Mascarene high) during its positive phase (Morioka et al. 2012). This strengthening of the Mascarene high may possibly inhibit TC formation due to suppression of convection which is intrinsic to cyclogenesis. Since teleconnections exhibit only quasi-periodic behavior at best, the resulting ensemble of three such indices is likely somewhat chaotic over time. This alone will cause TC statistics to be sensitive to the starting date and length of the averaging period (Henderson-Sellers et al. 1998; Mavume et al. 2009; Schreck et al. 2014). Figure 12 exhibits this complexity of year to year variations. 2005/2006 had the lowest number of observed TCs while the 2002/2003 season showed the highest. The anomalous low number of TCs in 2005/2006 were an all negative ENSO, IOD and SASD phase while

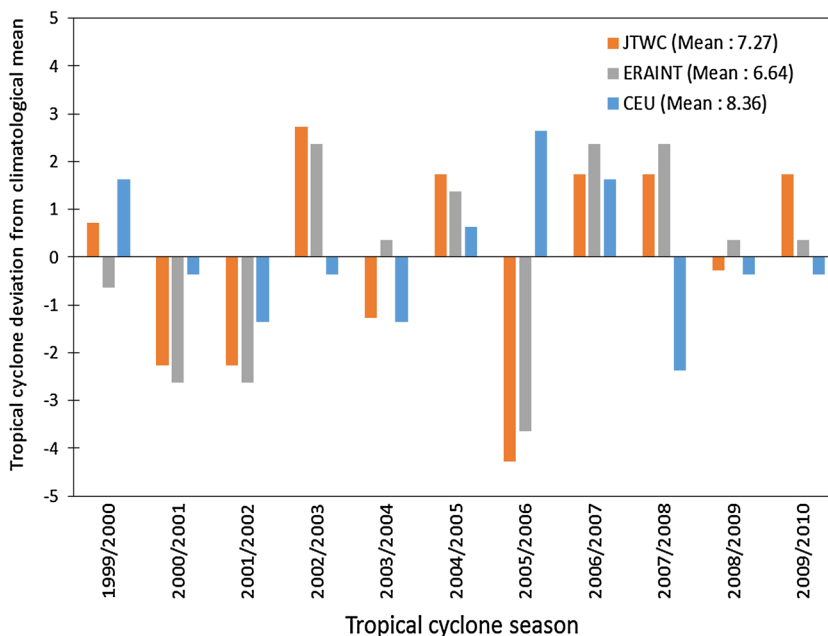
the 2002/2003 period had a positive ENSO and IOD but neutral SASD. CEU shows a large anomaly for 2005/2006 but in reverse in comparison to observation. Another CEU anomaly is in the 2007/2008 season which is marked by a positive IOD and SASD phase coupled with a negative ENSO mode. It is interesting to note that the high (low) CEU anomaly was simultaneous with negative (positive) IOD and SASD phase. However it is beyond the scope of this study to investigate what brings about these anomalous trends with regards to the SST indices.

ERAINT and CEU show an average of 6.6 and 8.1 TCs per year which is close the observed mean of 7 TCs per year. ERAINT captured the interannual variability of the JTWC data with a spearman correlation of $\rho=0.64$ and p value of 0.03. The corresponding numbers for CEU were $\rho = -0.50$ and $p=0.11$. This poor CEU correlation may be due to the 11-year record which is insufficient to evaluate the interannual variability. Twenty years is the minimum recommended by the World Meteorological Organization. However, Ensemble simulations could improve these results. Using phase synchronization (defined in Sect. 2.3.2), ERAINT showed better agreement ($\eta=73\%$) in comparison to CEU ($\eta=64\%$) with regards to the TC anomaly patterns in the observation (Fig. 12).

4 Conclusions

This study investigated the skill of a GCM with grid stretching (CEU) in simulating the characteristics of Tropical Cyclones (TCs) over the SWIO (South West Indian Ocean). The simulation was conducted over a period of

Fig. 12 Interannual variability of TC occurrence over the South West Indian Ocean for study period 1999–2010



11-years (1999–2010) for the SWIO TC Season (November–April). The model simulation was compared to JTWC observations and ERA-Interim (ERAINT) reanalysis data in order to evaluate the skill of the model in simulating the temporal and spatial variation of the regional climate over the SWIO. An objective TC tracking algorithm was used in order to detect and track TCs.

- In general, CEU shows good agreement with observations and ERAINT in simulating overall climatic features over the SWIO for the study period. However, compared to ERAINT, CEU simulation of the vorticity and rainfall has a notable discrepancy over the Mozambique Channel where CEU simulation of the vorticity and rainfall differ notably due to strong cyclonic features present in the CEU simulation over the region.
- The model and reanalysis reproduce well the spatial distribution of TC tracks over the SWIO but the model overestimate the number of TCs over the MC. CEU overestimates TC genesis over the MC. However they both CEU and ERAINT showed skill in simulating the spatial distribution of genesis locations.
- ERAINT and CEU adequately reproduce the essential dynamical structure of an observed TC, which consists of a warm core and well-defined eye surrounded by cyclonic winds that decay with increasing distance from the centre. A comparable storm was simulated by CEU with more detail in some aspects (particular in the rain bands) but was less deep in comparison to ERAINT.
- The ACE index for CEU is nearly twice that of ERAINT but still only about 50% of the JTWC data. Both ERAINT and CEU failed to capture the lowest MSLP of ~900 hPa in the observations. However CEU is closer to simulating these extreme values when compared to ERAINT (930 vs. 960 hPa).
- Both CEU and ERAINT reproduce well the monthly variation of TCs although TCs were overestimated for CEU during the peak months (i.e. January and February) in comparison to the observation. This is due to the strong vorticity bias over the MC which is favourable to tropical cyclogenesis. The model performed poorly in simulating the interannual variability of SWIO TCs.

The results of this study show that CEU has promise for seasonal forecasting over the SWIO. However, further development is planned to improve the performance of the model over the SWIO. The first improvement would be updating the CEU physics package from CAM3 to the newer CAM5.2, which offers improvements on the physics parameterizations. These improvements on parameterization schemes would hopefully improve the CEU simulation over the MC. Moreover, future studies are planned on studying the impacts of various parameterization schemes

on TCs over the SWIO, since moist processes have been shown to play an important role in strengthening TCs. In addition, to address uncertainty in observation of TC tracking, future study would use more than one observation datasets in evaluating the model results.

Potential work following from this study should also consider performing ensemble runs in order to provide a more robust climatological analysis of the SWIO, which may improve the TC simulation statistics over the basin. Another possible study could also look at the comparison of uniform grid vs. stretched-grid on TC characteristics. In this study, TCs were simulated using a static stretch grid but the next planned study will look at dynamic grid stretching, which allows for dynamic tracking of features of interest (e.g. storms) whilst increasing resolution locally.

Acknowledgements The project was supported with grants and bursaries from National Research Foundation (NRF, South Africa), Water Research Commission (WRC, South Africa), and the Future Resilience for African Cities and Lands (FRACTAL) project. Computing facility was provided by Centre for High Performance Computing (CHPC, South Africa). We thank the two anonymous reviewers, whose comments have helped in improving the quality of the manuscript.

References

- Abiodun BJ, Prusa JM, Gutowski WJ Jr (2008) Implementation of a non-hydrostatic, adaptive-grid dynamics core in CAM3. Part I: comparison of dynamics cores in aqua-planet simulations. *Clim Dyn* 31(7–8):795–810
- Abiodun BJ, Gutowski WJ, Abatan AA, Prusa JM (2011) CAM-EULAG: a non-hydrostatic atmospheric climate model with grid stretching. *Acta Geophys* 59(6):1158–1167
- Araujo JA, Abiodun BJ, Crespo O (2014) Impacts of drought on grape yields in Western Cape, South Africa. *Theoret Appl Climatol*, pp 1–14
- Badarinath KVS, Mahalakshmi DV, Ratna SB (2012) Influence of land use land cover on cyclone track prediction—a study during Ailia cyclone. *Open Atmos Sci J* [Online] 6:6 February 2013. Available from: <http://benthamopen.com/toascj/articles/V006/33TOASCJ.pdf>
- Bell GD, Halpert MS, Schnell RC, Higgins RW, Lawrimore J, Kousky VE, Tinker R, Thiaw W, Chelliah M, Artusa A (2000) Climate assessment for 1999. *Bull Am Meteorol Soc* 81(6):s1–s50
- Bell J, Hodges K, Vidale PL, Strachan J, Roberts M (2014) Simulation of the global ENSO–tropical cyclone teleconnection by a high-resolution coupled general circulation model. *J Clim* [Online] 27(17):14 (November 2014-6404-6422). Available from: <http://journals.ametsoc.org/doi/pdf/10.1175/JCLI-D-13-00559.1>
- Bengtsson L, Botzet M, Esch M (1995) Hurricane-type vortices in a general circulation model. *Tellus* [Online] 47A(2):175–196. Available from: http://envsci.rutgers.edu/~toine379/extremeprecip/papers/bengtsson_et_al_1995.pdf. 4 Nov 2014
- Bengtsson L, Botzet M, Esch M (1996) Will greenhouse gas-induced warming over the next 50 years lead to higher frequency and greater intensity of hurricanes?. *Tellus* [Online], 4A(1):3 November 2014-57-73. Available from: <http://pubman.mpdl.mpg.de/pubman/item/escidoc:1852493:2/component/escidoc:1852573/11632-38420-1-SM.pdf>

- Berrisford P, Kallberg P, Kobayashi S, Dee D, Uppala S, Simmons A, Poli P, Sato H (2011) The ERA-Interim archive version 2.0. Eur Centre Medium-Range Weather Forecasts ERA Tech Rep 1:23
- Caian M, Geleyn JF (1997) Some limits to the variable-mesh solution and comparison with the nested lam solution. *Q J R Meteorol Soc* 123(539):743–766
- Camargo SJ, Sobel AH (2005) Western North Pacific tropical cyclone intensity and ENSO. *J Clim* 18(15):2996–3006
- Chatzidimitriou K, Sutton A (2005) Alternative data mining techniques for predicting tropical cyclone intensification. In: American Association for Artificial Intelligence, vol 37. Citeseer, New Jersey, pp 99–128
- Collins WD, Rasch PJ, Boville BA, Hack JJ, McCaa JR, Williamson DL, Kiehl JT, Briegleb B, Bitz C, Lin S (2004) Description of the NCAR community atmosphere model (CAM 3.0)”
- Driver P (2014) Rainfall variability over Southern Africa, PhD Thesis Submitted to the University of Cape Town
- Dvorak VF (1984) Tropical cyclone intensity analysis using satellite data, US Department of Commerce, National Oceanic and Atmospheric Administration, National Environmental Satellite, Data, and Information Service
- Girishkumar MS, Ravichandran M (2012) The influences of ENSO on tropical cyclone activity in the Bay of Bengal during October–December. *J Geophys Res* 117:C02033. doi:10.1029/2011JC007417
- Goerss JS (2000) Tropical cyclone track forecasts using an ensemble of dynamical models. *Mon Weather Rev* 128(4):1187–1193
- Gray WM (1968) “Global view of the origin of tropical disturbances and storms. *Mon Weather Rev* 96(10):669–700
- Gray WM (1979) Hurricanes: their formation, structure, and likely role in the tropical circulation. In: Shaw DB (ed) *Meteorology over the Tropical Oceans*. Royal meteorological Society, pp 155–218
- Hamill TM, Whitaker JS, Fiorino M, Benjamin SG (2011) Global ensemble predictions of 2009’s tropical cyclones initialized with an ensemble Kalman filter. *Mon Weather Rev* 139(2):668–688
- Harris LM, Lin SJ, Tu C (2016) High-resolution climate simulations using GFDL HiRAM with a stretched global grid. *J Clim* 29(11):4293–4314
- Hashimoto A, Done JM, Fowler LD, Bruyère CL (2016) Tropical cyclone activity in nested regional and global grid-refined simulations. *Clim Dyn* 47(1–2):497–508
- Henderson-Sellers A, Zhang H, Berz G, Emanuel K, Gray W, Landsea C, Holland G, Lighthill J, Shieh S, Webster P (1998) Tropical cyclones and global climate change: a post-IPCC assessment. *Bull Am Meteorol Soc* 79(1):19–38
- Holland GJ (1993) Ready reckoner. *Glob Guide Trop Cyclone Forecast*, pp 9–1
- IRIN, Tropical Cyclone Haruna hits southwestern Madagascar. 2015, [Homepage of IRINNews], [Online]. Available: <http://www.irin-news.org/report/97542/tropical-cyclone-haruna-hits-southwestern-madagascar> [2015, April]
- Kleppik S, Muccione V, Raible CC, Bresch DN, Koellner-Heck P, Stocker TF (2008) Tropical cyclones in ERA-40: a detection and tracking method. *Geophys Res Lett* 35:L10705. doi:10.1029/2008GL033880
- Klinman M, Reason C (2008) On the peculiar storm track of TC Favio during the 2006–2007 Southwest Indian Ocean tropical cyclone season and relationships to ENSO. *Meteorol Atmos Phys* 100(1–4):233–242
- Kurowski MJ, Grabowski WW, Smolarkiewicz PS (2014) Anelastic and compressible simulation of moist deep convection. *J Atmos Sci* 71:3767–3787
- Kurowski MJ, Grabowski WW, Smolarkiewicz PS (2015) Anelastic and compressible simulation of moist dynamics at planetary scales. *J Atmos Sci*, V72:3975–3995
- LaRow TE, Lim YK, Shin DW, Chassignet EP, Cocke S (2008) Atlantic basin seasonal hurricane simulations. *J Clim* 21(13):3191–3206
- Manabe S, Holloway JL Jr, Stone HM (1970) Tropical circulation in a time-integration of a global model of the atmosphere. *J Atmos Sci* 27(4):580–613
- Mavume FA, Rydberg L, Rouault M, Lutjeharms REJ (2009) Climatology and landfall of tropical cyclones in the South West Indian Ocean. *West Indian Ocean J Mar Sci* 8(1):15–36
- Mbedzi MP (2010) Simulation of tropical cyclone-like vortices over the southwestern Indian Ocean, University of Pretoria
- Misra J (1991) Phase synchronization. *Inf Process Lett* 38(2):101–105
- Morioka Y, Tozuka T, Masson S, Terray P, Luo J, Yamagata T (2012) Subtropical dipole modes simulated in a coupled general circulation model. *J Clim* 25(12):4029–4047
- National Weather Service, Tropical Cyclone Structure. 2010, [Homepage of National Weather Service], [Online]. Available: http://www.srh.noaa.gov/jetstream/tropics/tc_structure.htm?&sessionId=e2221f2646ce61f563e3a28f1ec4d98. 2015, July
- Ogier D (2013) Characteristics of inertial gravity waves over Southern Africa as simulated with CAM-EULAG, A MSc thesis submitted to the University of Cape Town
- Prusa JM, Gutowski WJ (2010) Multi-scale waves in sound-proof global simulations with EULAG. *Acta Geophys V59*:1135–1157
- Rodrigues RR, Campos EJ, Haarsma R (2015) The impact of ENSO on the South Atlantic subtropical dipole mode. *J Clim* 28(7):2691–2705
- Saha KK, Wasimi SA (2013) Interrelationship between Indian Ocean Dipole (IOD) and Australian Tropical Cyclones. *Int J Environ Sci Dev* 4(6):647
- Saji N, Goswami BN, Vinayachandran P, Yamagata T (1999) A dipole mode in the tropical Indian Ocean. *Nature* 401(6751):360–363
- Schenkel BA, Hart RE (2012) An examination of tropical cyclone position, intensity, and intensity life cycle within atmospheric reanalysis datasets. *J Clim* 25(10):3453–3475. doi:10.1175/2011JCLI4208.1
- Schreck CJ III, Knapp KR, Kossin JP (2014) The impact of best track discrepancies on global tropical cyclone climatologies using IBTrACS. *Mon Weather Rev* 142(10):3881–3899
- Strachan J, Vidale PL, Hodges K, Roberts M, Demory M (2013) Investigating global tropical cyclone activity with a hierarchy of AGCMs: The role of model resolution. *J Clim* [Online] 26(1):5 November-133-152. Available from: <http://journals.ametsoc.org/doi/pdf/10.1175/JCLI-D-12-00012.1>
- Tozuka T, Abiodun BJ, Engelbrecht FA (2014) Impacts of convection schemes on simulating tropical-temperate troughs over southern Africa. *Clim Dyn* 42(1–2):433–451
- Vitart F, Anderson J, Stern W (1997) Simulation of interannual variability of tropical storm frequency in an ensemble of GCM integrations. *J Clim* 10(4):745–760
- Vitart F, Anderson D, Stockdale T (2003) Seasonal forecasting of tropical cyclone landfall over Mozambique. *J Clim* 16(23):3932–3945
- Walsh K, Fiorino M, Landsea C, McInnes K (2007) Objectively determined resolution-dependent threshold criteria for the detection of tropical cyclones in climate models and reanalyses. *J Clim* 20(10):2307–2314
- Walsh KE, Camargo SJ, Vecchi GA, Daloz A, Elsner J, Emanuel K, Horn M, Lim Y, Roberts M, Patricola C, Scoccimarro E, Sobel AH, Strazzo S, Villarini G, Wehner M, Zhao M, Kossin JP, LaRow T, Oouchi K, Schubert S, Wang H, Bacmeister J, Chang P, Chauvin F, Jablonowski C, Kumar A, Murakami H, Ose T, Reed KA, Saravanan R, Yamada Y, Zarzycki CM, Vidale P, Jonas JA, Henderson N (2015) Hurricanes and climate: the U.S. CLIVAR working group on hurricanes. *Bull Am Meteorol Soc* 96:997–1017. doi:10.1175/BAMS-D-13-00242.1

- Williamson DL (2008) Convergence of aqua-planet simulations with increasing resolution in the Community Atmospheric Model, Version3. *Tellus* 60A:848–862
- Zarzycki CM, Jablonowski C (2014) A multidecadal simulation of Atlantic tropical cyclones using a variable resolution global atmospheric general circulation model. *J Adv Model Earth Syst* 6(3):805–828
- Zarzycki CM, Jablonowski C, Taylor MA (2014) Using variable-resolution meshes to model tropical cyclones in the Community Atmosphere Model. *Mon Weather Rev* 142(3):1221–1239
- Zhao M, Held IM (2012) TC-Permitting GCM simulations of hurricane frequency response to sea surface temperature anomalies projected for the late-twenty-first century. *J Clim* [Online] 24(8):15 (November 2014-2995-3009). Available from: <http://journals.ametsoc.org/doi/pdf/10.1175/JCLI-D-11-00313.1>